The 11th Canadian Conference on Earthquake Engineering
Canadian Association for Earthquake Engineering

RESTORING FORCE CHARACTERISTICS MODEL OF CES SHEAR WALLS

Suguru SUZUKI
Assistant Professor, OSAKA UNIVERSITY, JAPAN
suzuki@arch.eng.osaka-u.ac.jp

Hiroshi KURAMOTO
Professor, OSAKA UNIVERSITY, JAPAN
kuramoto@arch.eng.osaka-u.ac.jp

ABSTRACT: CES structures composed of steel and fiber reinforced concrete have been continuously studied by the authors. Since CES structural system is a new composite structural system, it is expected to design by Capacity Spectrum Method with pushover analysis or the time history response analysis. In this study, a non-linear static analysis for CES shear walls with different anchorage condition of longitudinal wall reinforcing bars was conducted to verify the validity of the analytical modeling. The analytical results for the shear force versus drift angle relationships and the deformation behavior of each component showed good agreement with the experimental results. It was also indicated that the different anchorage method of longitudinal wall reinforcing bars affects little on the hysteretic characteristics of CES shear walls.

1. Introduction

The authors have continuously conducted a study on composite Concrete Encased Steel (CES) structural systems composed of steel and fiber reinforced concrete (FRC).

CES frames can be used larger cross section steels than those in SRC frames, since the CES members are not arranged reinforcing bars. Therefore, CES shear walls can resist shear forces, because the wall panel is confined by sturdy boundary columns with a full-web steel. From the results of experiment (Suzuki, et al., 2012) and FEM analysis (Suzuki, et al., 2014), it was confirmed that the deformability of CES shear walls improves by omitting the anchorage of longitudinal wall reinforcement.

On the other hands, since CES structural system is a new composite structural system, it is expected that the structural performance of the structures are evaluated by Capacity Spectrum Method using pushover analysis or the time history response analysis. In these analyses, shear walls are generally replaced by Three Vertical Line Elements (TVLE) model (Kabeyasawa, et al, 1987). TVLE model is an effective tool for nonlinear analysis if it is possible to provide adequate restoring force characteristics of each component in a shear wall such as boundary columns and a wall panel.

This study aimed at developing the restoring force characteristics model of CES shear walls to the structural performance evaluation method, which is applied. A non-linear static analysis with TVLE model was conducted to verify the validity of the analytical model of CES shear walls with different anchorage condition between the wall and the surrounding CES frame.

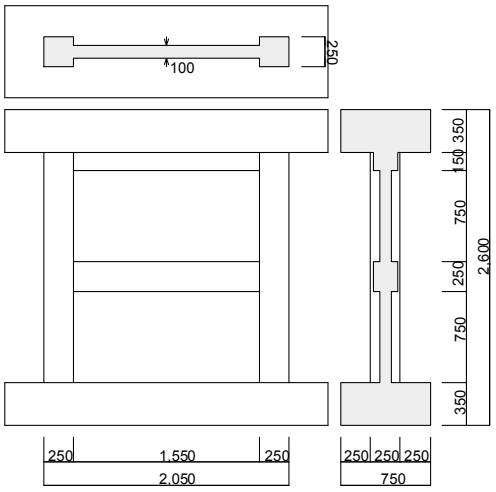

Fig. 1 - Test Specimen

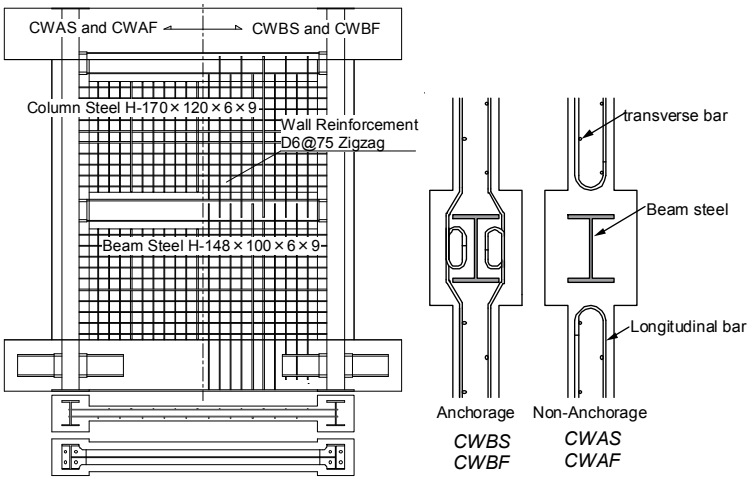

Fig. 2 - Bar Arrangement

Table 1 - Details of Specimens

Specimens		*CWAS*	*CWAF*	*CWBS*	*CWBF*
Column	*BxD*	250x250 (mm)			
	Steel	H-170x120x6x9 ($_sp$=4.9%)			
Beam	*BxD*	200x250 (mm)			
	Steel	H-148x100x6x9 ($_gp$=5.2%)			
Wall	Thickness	100 (mm)			
	Longitudinal bar	D6@75 zigzag ($_wp$=0.42%)			
	Transverse bar				
Shear span ratio		1.1	1.65	1.1	1.65
Anchorage condition of longitudinal wall reinforcement		Non-existent		180° hook in beam	

2. Test of CES shear walls

2.1. Specimens

A total of four specimens were designed to simulate the lower two stories of a multi-story shear wall in a medium rise building, which were one-third scale of the prototype walls. The configurations and bar arrangements of the specimens are shown in Figs. 1 and 2. Details of the cross sections are shown in Table 1. The boundary column had a 250mm square section, and the beam section was 200x250mm. The column span length was 1,800mm, and the wall thickness was 100mm. The variables investigated were the shear-span ratio and the anchorage condition of longitudinal wall reinforcing bars. The shear-span ratio was 1.1 for Specimens CWAS and CWBS, and 1.65 for Specimens CWAF and CWBF. Specimens CWAS and CWBS were expected to be shear failure mode, while Specimens CWAF and CWBF were expected to be flexural failure mode. The longitudinal wall reinforcing bars for Specimens CWAS and CWAF were bent in wall panel. On the other hand, the longitudinal wall reinforcing bars for Specimens CWBS and CWBF were anchored to a beam and stubs, as shown in Fig. 2. The transverse wall reinforcing bars in all specimens were securely fixed by welding them to the steel web in the CES boundary columns. In addition, the H-section steels of the boundary columns were anchored to the upper and lower stubs in all specimens.

The mechanical properties of the FRC and steel used are shown in Tables 2 and 3, respectively. Poly vinyl alcohol (PVA) fibers with a diameter of 0.66mm and a length of 30mm were used for the FRC. The volumetric ratio of the fibers was 1.0%.

Table 2 - Mechanical Properties of FRC

Specimen		σ_B (N/mm^2)	E_C (kN/mm^2)	ε_{c0} (μ)
CWAS	1st story	38.6	24.8	2,814
	2nd story	36.4	26.7	2,550
CWBS	1st story	42.0	25.7	2,587
	2nd story	30.6	29.5	2,558
CWAF	1st story	41.2	25.5	2,457
	2nd story	38.6	27.6	2,423
CWBF	1st story	40.1	24.9	2,765
	2nd story	35.9	24.8	3,160

Table 3 - Mechanical Properties of Steel

	σ_y (N/mm^2)	E_s (kN/mm^2)	σ_u (N/mm^2)
PL-6 (SS400)	260	190	409
PL-9 (SS400)	282	197	418
D6 (SD295A)	345	190	501

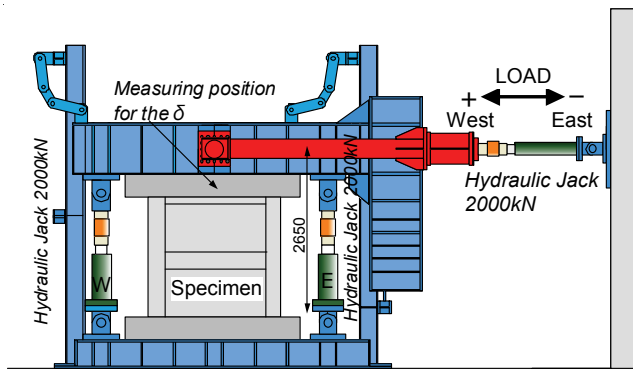

Fig. 3 - Loading Apparatus

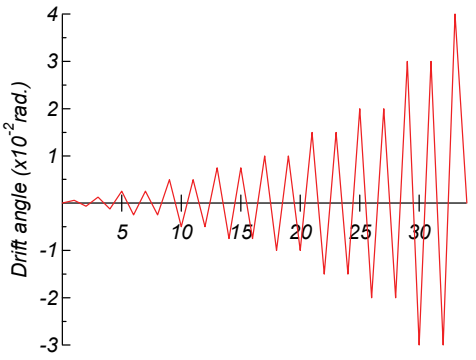

Fig. 4 - Loading Protocol

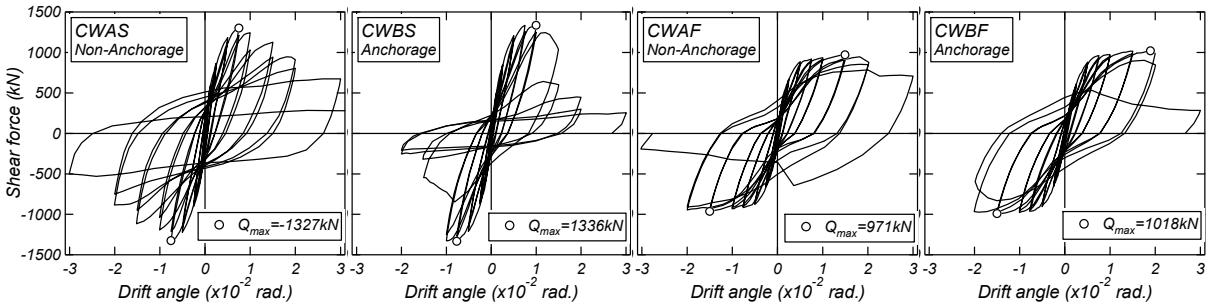

Fig. 5 – Shear Force - Drift Angle Relationships

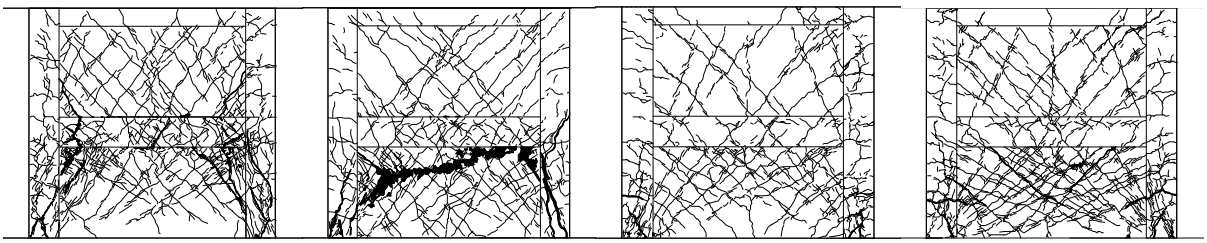

CWAS **CWBS** **CWAF** **CWBF**

Fig. 6 – Cracking Pattern at R of 1.5 x 10^{-2} rad.

2.2. Loading Program

Figure 3 shows the loading apparatus. The specimens were loaded horizontal cyclic shear forces using a hydraulic jack with a 2,000kN capacity, while applying a constant axial force of 1,260kN (N/N_0=0.2, where N=axial load, N_0=axial load capacity including steel of boundary columns) using two vertical hydraulic jacks, each of which had a 2,000kN capacity. During the testing, additional moment was also applied to the top of the specimen using the two vertical jacks to maintain the prescribed shear-span ratio of 1.1 or 1.65.

Figure 4 shows the loading protocol. The loading was conducted by controlling the relative drift angle, R, given by the ratio of the height corresponding to the measuring point for the horizontal displacement at the top of the specimen, h_0 (2,050 mm), to the horizontal deformation, δ, i.e., $R=\delta/h_0$.

2.3. Experimental Results

The shear force-drift angle relationships and the cracking patterns at R=1.5 x 10^{-2} rad. for all specimens are shown in Figs. 5 and 6, respectively. In Fig. 5, circles show the point of the maximum capacities in both positive and negative loadings.

The maximum capacities of Specimens CWAS and CWBS, which have shear failure, were almost the same. However, the deformability of the specimens were different after reaching the maximum capacity. The shear force of Specimen CWAS decreased slowly, while that of Specimen CWBS decreased drastically at R of 1.5 x 10^{-2} rad.

The horizontal slip between wall panel and beam versus drift angle relationships of shear failure specimens are shown in Fig. 6. In Specimens CWBS with longitudinal wall reinforcement anchorage, the horizontal slip between wall panel and beam hardly occurred. However, in Specimen CWAS without longitudinal wall reinforcement anchorage, the horizontal slip between wall panel and beam increased at R of 1.0 x 10^{-2} rad. This reason is because the damage of wall panel in Specimen CWAS is less than that in Specimen CWBS due to the development of slip between wall panel and beam in Specimen CWAS.

The maximum capacities of two specimens CWAF and CWBF are almost the same. These specimens showed significant strength deterioration in the loading cycle of 3.0 x 10^{-2} rad. However, the deformability of Specimen CWBF was slightly poorer than that of Specimen CWAF.

Thus, it is found that the anchorage condition for the longitudinal wall reinforcement had little effect on the maximum capacity. In addition, the deformability can be improved by omitting the anchorage of the longitudinal wall reinforcement.

3. Modeling of Restoring force Characteristics

3.1. Outline of the analysis model

A non-linear analysis was conducted for the CES shear walls using the commercial software “SNAP”. Analytical model is shown in Fig. 7. CES shear wall was adopted as TVLE models which was composed of two truss elements representing boundary columns and a beam element representing wall panel as shown in Fig. 7. Specimens were modeled to each story. The elements between a loading point prescribe shear span ratio of 1.1 or 1.65 and the top end of upper stub were assumed to be rigid. A node at the top of the virtual stub was subjected to lateral displacement reversals with applying a constant axial force of 1,260kN. Each node at the bottom end of the column in 1st story was fixed to restrain displacement. In addition, analytical results were shown until the loading cycle at reaching the maximum capacity in the test.

3.2. Restoring Force Characteristics

The backbone curve of flexural moment-curvature relationships in wall panel was expressed as tri-linear, as shown in Fig. 8(a). It was assumed that the plastic hinge was formed in the bottom of wall panel. The first point was expressed as flexural cracking point. The moment M_{cr} and curvature φ_{cr} were calculated using Eqs. 1 and 2. The second point was expressed as yielding point of column steel. The moment M_u was calculated using Eq. 3. However, in the calculation results of Specimens CWAS and CWAF without anchorage, the effects of longitudinal wall reinforcement was ignored. The curvature φ_u was calculated by the fiber section analysis. Axial force N_w in the analysis was a load applied for the corresponding section area of wall panel. Takeda model with unloading stiffness coefficient of 0.4 was used for the hysteretic model, as shown in Fig. 8(a)

$$M_{cr} = \left(0.56\sqrt{\sigma_B} + \frac{N_w}{{}_{we}A} \right) Z_{we} \tag{1}$$

$$\phi_{cr} = \frac{M_{cr}}{E_c \cdot I_{we}} \tag{2}$$

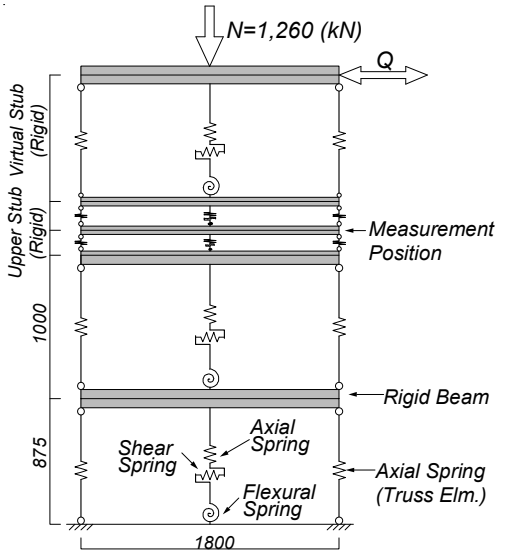

Fig. 7 - Analytical Model

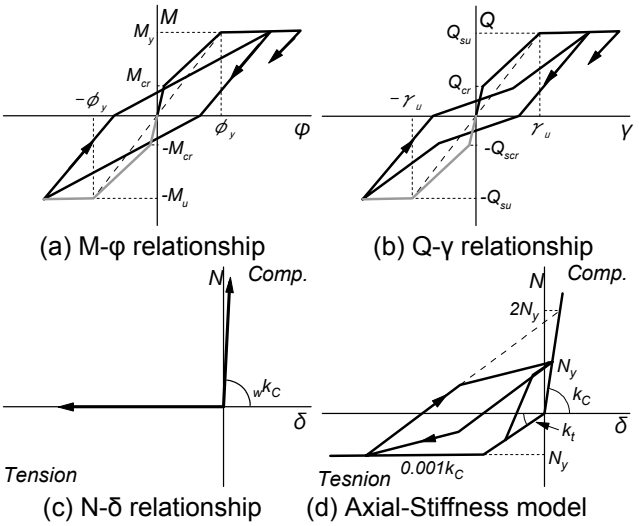

Fig. 8 - Restoring for Characteristics Model

$$M_u = 0.4_{mw}A\cdot_m \sigma_y \cdot l' + 0.5N_w \cdot l'\left(1 - \frac{N_w}{{}_wt \cdot l' \cdot \sigma_B}\right) \quad (3)$$

where $_{we}A$ is Equivalent section area of wall panel, Z_{we} is equivalent section modulus of wall panel, E_c is young's modulus of concrete, I_{we} is equivalent moment of inertial of area of wall panel, and l' is length of wall panel.

The backbone curve of shear force-shear strain relationships in wall panel was expressed by tri-linear. The first point was expressed as shear cracking point. The strength Q_{cr} was calculated using Eq. 4 and te strain γ_{cr} was calculated using Eq. 5. The second point was expressed as the ultimate strength point. The strength Q_{su} was calculated using the Truss-Arch equation (Eq. 6) (Suzuki, et. al., 2014). The strain γ_u (Eq. 7) was calculated by Sugano Equation β_u (Eq. 8) (Sugano, 1973). Takeda-Slip model with unloading stiffness coefficient of 0.5 was used for the hysteretic model, as shown in Fig. 8(b).

$$Q_{scr} = \sqrt{\sigma_{cr}\left(\sigma_{cr} + \sigma_0\right)}{}_wt\cdot_w l / \kappa_s \quad (4)$$

$$\gamma_{cr} = Q_{scr} \cdot \kappa_e / \left(G_c\cdot_w t\cdot_w l\right) \quad (5)$$

where σ_{cr} is cracking strength of concrete (=0.33$\sqrt{\sigma_B}$), σ_0 is axial stress at constant axial force, κ_s is shape coefficient (=1.17), D is depth of column. κ_e is shape coefficient of rectangular cross-section (=1.2), G_c is shear modulus of concrete, $_wt$ is wall thickness, and $_wl$ is column span length.

$$Q_{su} = {}_wt\left\{{}_wl_t \cdot p_{se}\cdot_w \sigma_y \cot\phi + \tan\theta\left(1-\beta\right){}_wl_a \cdot \nu \cdot \frac{\sigma_B}{2}\right\} \quad (6)$$

$$\gamma_{su} = Q_{su} / \left(\beta_u \cdot G_c\cdot_w t\cdot_w l\right) \quad (7)$$

$$\beta_u = 0.46\frac{{}_w\sigma_y\cdot_w p}{\sigma_B} + 0.14 \quad (8)$$

where $_wl_t$ is wall length of truss mechanism, p_{se} is ratio of horizontal wall reinforcement including a lower flange of beam steel, $_w\sigma_y$ is yield strength of horizontal wall reinforcement, φ is angle of concrete compression strut of truss mechanism (cotφ=1), θ is angle of concrete compression strut of arch mechanism, β is shear contribution ratio of truss mechanism, $_wl_a$: wall length of arch mechanism, v is compressive strength reduction factor of concrete (=0.7-σ_B/200), and $_wp$ is ratio of horizontal wall reinforcement.

The backbone curve of axial force-axial displacement relationships in wall panel for Specimens CWAS and CWAF without the anchorage of longitudinal reinforcement was shown in Fig. 8(c). That for Specimens CWBS and CWBF with the anchorage was expressed by Axial-Stiffness model, as shown in Fig. 8(d). The elastic stiffness in compression ${}_wk_c$ was calculated using Eq. 9. The first point in tension of Axial-Stiffness model (Kabeyasawa, 1983) was expressed as yielding point of wall reinforcing bars. The yield strength ${}_wN_y$ and stiffness ${}_wk_t$ were calculated using Eqs. 10 and 11.

$$ {}_wk_c = {}_{we}A \cdot E_c / h_w \tag{9} $$

$$ {}_wN_y = {}_{mw}A \cdot {}_m\sigma_y \tag{10} $$

$$ {}_wk_t = {}_{mw}A \cdot E_{ws} / h_w \tag{11} $$

where ${}_{we}A$ is equivalent section area of wall panel, h_w is story height, ${}_{mw}A$ is area of longitudinal wall reinforcement, ${}_m\sigma_y$ is yield strength of longitudinal wall reinforcement, and E_{ws} is young's modulus of wall reinforcing bars.

The backbone curve of axial force-axial displacement relationships in boundary column was expressed by Axial-Stiffness model, as shown in Fig. 8(c). The elastic stiffness in compression ${}_ck_c$ was calculated using Eq. 12. The first point in tension was expressed as the yielding point of steel in column. The strength ${}_cN_y$ and stiffness ${}_ck_t$ were calculated using Eqs. 13 and 14.

$$ {}_ck_c = {}_{ce}A \cdot E_c / h_w \tag{12} $$

$$ {}_cN_y = {}_{cs}A \cdot {}_s\sigma_y \tag{13} $$

$$ {}_ck_t = {}_{cs}A \cdot E_s / h_w \tag{14} $$

where ${}_{ce}A$ is equivalent section area of boundary column, ${}_{cs}A$ is area of column steel, ${}_s\sigma_y$ is yield strength of column steel, and E_s is young's modulus of boundary column steel.

4. Analytical Results

4.1. Backbone Curves

Figure 9 shows comparisons between test and analytical results on backbone curves. For Specimens CWAF and CWBF, the stiffness before the yielding point of column steel for the analysis was larger than that for the test. For these specimens, as shown in Fig. 10, the maximum flexural crack width between boundary column and bottom stub in the 1st-story increased at R of 0.5 x 10^{-2} rad. before yielding of steel in boundary column. Additional deformations caused by the flexural crack occurred because the bond action between steel and concrete cannot be expected in the CES shear walls with H-shaped steel in boundary columns. Therefore, the initial stiffness of boundary column in tension was reduced by half of the stiffness of steel by trial and error method.

Figure 11 shows backbone curves of analytical results which were reduced by half the elastic stiffness in tension. The yielding point of column steel and the ultimate shear strength point of wall panel in analytical results showed good agreements with those in the test results for all specimens.

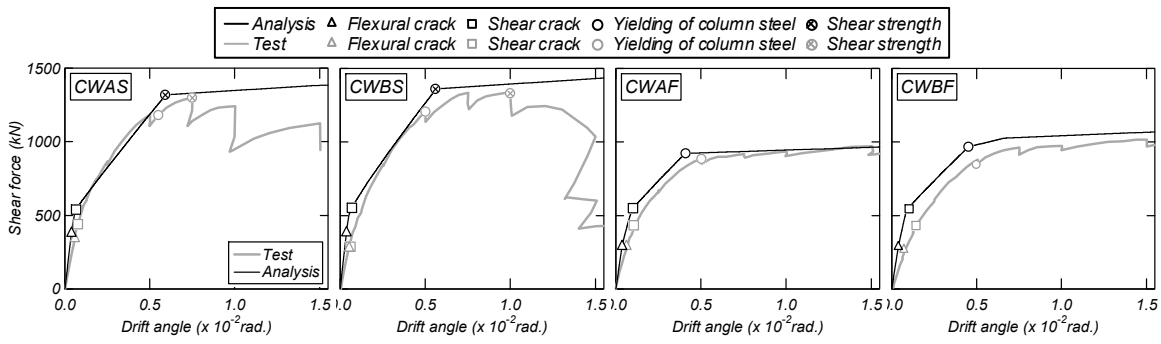

Fig. 9 - Comparisons between Analysis and Experimental Results

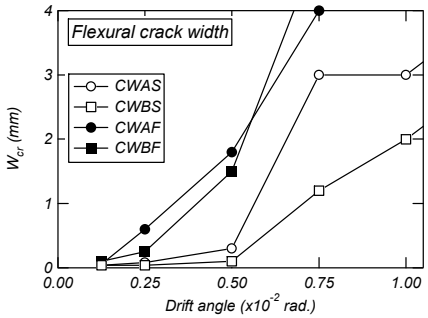

Fig. 10 – Transitions of Flexural Crack Width between Column and Stub at Bottom in 1-Story

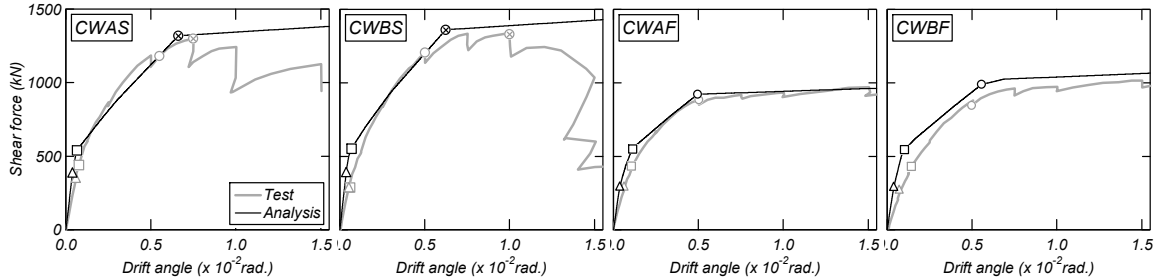

Fig. 11 – analytical results of a half elastic stiffness in tension

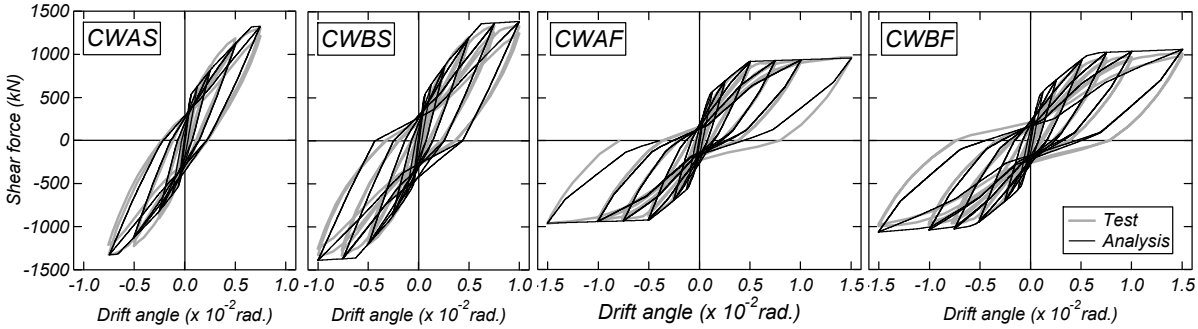

Fig. 12 – Comparisons between Experimental and Analytical results on Hysteretic Characteristics

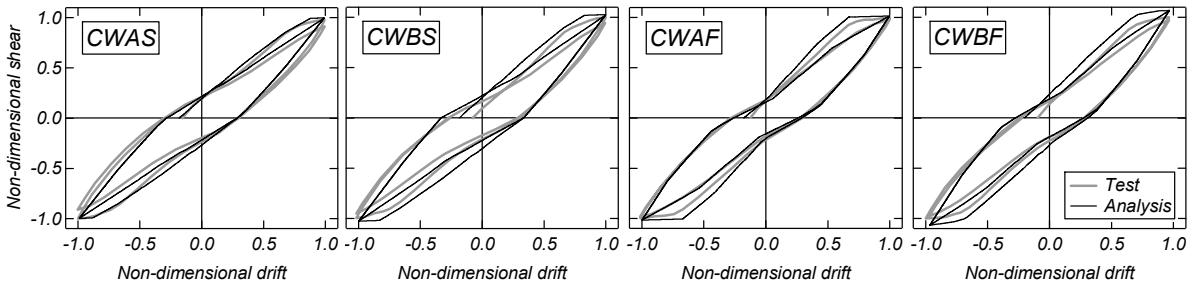

Fig. 13 – Non-Dimensional Shear-Drift Relationships in Cycle of 0.75 x 10^{-2} rad.

4.2. Hysteretic Characteristics

Figure 12 shows comparisons between test and analytical results on hysteretic characteristics, while Figure 13 shows non-dimensional shear-drift relationships in the loading cycle of 0.75 x 10^{-2} rad.

In Specimens CWAS and CWBS with shear failure, both analytical and test results after R of 0.75 x 10^{-2} rad. showed slip-typed hysteresis loops. In Specimens CWAF and CWBF with flexural failure, the

absorbed energy after R of 1.5 x 10^{-2} rad. in the analysis was smaller than that in the test. However, analytical results before R of 1.5 x 10^{-2} rad. showed good agreement with test results. Moreover, the effect of the different anchorage condition of longitudinal wall reinforcing bars on hysteretic behavior was small between test and analytical results.

4.3. Deformation Components

Figure 14 shows the relationships between shear force and separated horizontal deformation components in Specimens CWAS and CWAF. Each component was defined as follows; flexural deformations in the 1st and 2nd stories, δ_{1f} and δ_{2f}, shear deformations in the 1st and 2nd stories, δ_{1s} and δ_{2s}, and rotational deformation in the 2nd story caused by flexural deformation in the 1st story, δ_{2r},. Figure 15 shows the measurement for the displacement. The flexural deformations, δ_{1f} and δ_{2f} (Eqs. 15 and 16) and the rotational deformation, δ_{2r} (Eq.17) were obtained by integrating rotation angle θ_i, where θ_i was calculated by axial displacements along with boundary columns, with respect to the height of specimen. The shear deformations, δ_{1s} and δ_{2s} were obtained by subtracting the flexural deformation from total story deformation in each story (Eqs. 18 and 19).

$$\delta_{1f} = \sum_{i=1}^{3}\left[\frac{\theta_i \cdot a_i}{2} + \theta_i\left(h_1 - \sum_{j=1}^{i} a_j\right)\right] \quad (15)$$

$$\delta_{2f} = \sum_{i=4}^{7}\left[\frac{\theta_i \cdot a_i}{2} + \theta_i\left(h_2 - \sum_{j=4}^{i} a_j\right)\right] \quad (16)$$

$$\delta_{2r} = \sum_{i=1}^{3} \theta_i \cdot h_2 \quad (17)$$

$$\delta_{1s} = \delta_1 - \delta_{1f} \quad (18)$$

$$\delta_{2s} = \delta_2 - \left(\delta_{1f} + \delta_{1s} + \delta_{2f} + \delta_{2r}\right) \quad (19)$$

where a_i and a_j are length of each measurement interval, h_1 and h_2 are measurement height of horizontal displacement in each-story.

For Specimen CWAS, It is seen that the shear deformations in the 1st and 2nd stories increased significantly in both analytical and test results and the analytical results showed good agreement with test results. However, the flexural deformation of the 1st story in the analysis was slightly smaller than that in the test. For Specimen CWAF with flexural failure, on the other hand, analytical results can simulate well not only the flexural deformation

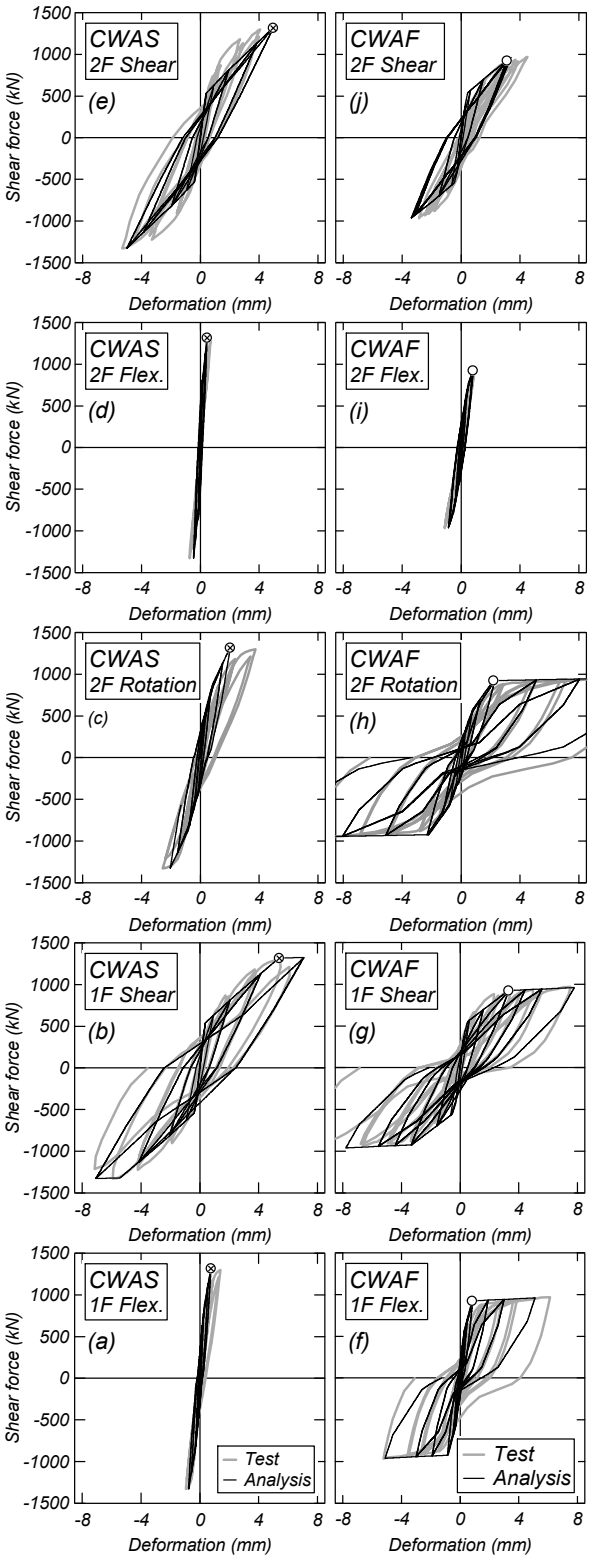

Fig. 14 – Shear force-each deformation relationships (left: CWAS, right: CWAF)

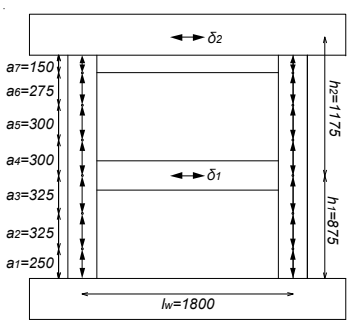

Fig. 15 – Measurement Position

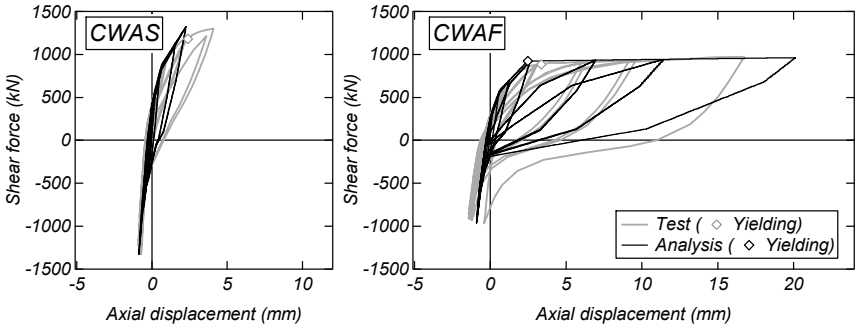

Fig.16 – Shear Force-Axial Displacement relationships

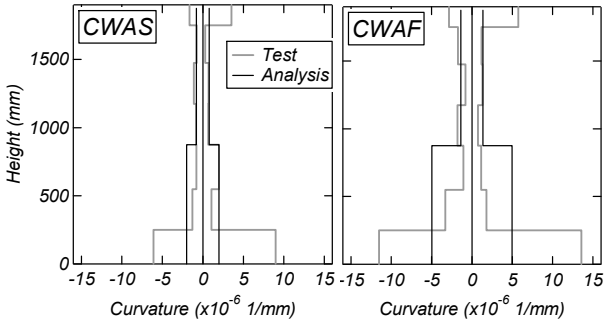

Fig. 17 – Curvature Distribution (R=0.75 × 10^{-2} rad.)

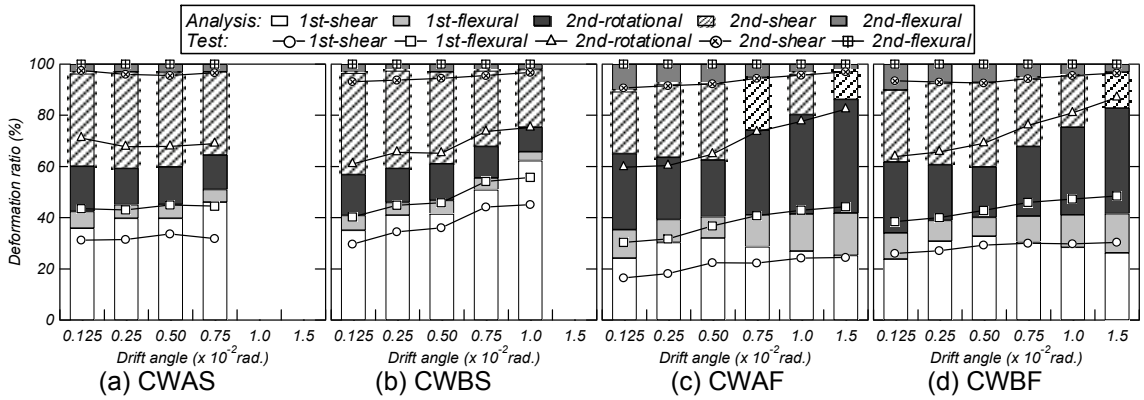

Fig. 18 – Ratios of each deformation components between analysis and experiment

but also the shear and rotational deformations in the test results.

Figure 16 shows the shear force-axial deformation relationship of boundary column in the 1st story. In Specimen CWAS with shear failure, the tensile deformation in the analysis was smaller than that in the test in final loading cycle. Moreover, column steels in the test yielded, while those in the analysis did not yield. This is caused by the different curvature distributions between the analysis and test, as shown in Fig. 17. The curvature in the test was increased at bottom in the 1st story while that assumed in the analysis was constant in each story. Then, the yielding of column steel was not observed in the analysis. On the other hand, in Specimen CWAF with flexural failure, the curvature at the bottom in the analysis was smaller than that in the test. However, the tensile deformation in the analysis was larger than that in the test due to overestimation of the constant curvature distribution in the 1st story in the analysis.

Figure 18 shows the ratios of separated horizontal deformation components at the peak in each loading cycle between analysis and test. In the specimens with shear failure, the transition of the ratios of

deformation components with increasing the drift angle, R, in the test for Specimen CWAS without the anchorage was almost constant before R of 0.75 x 10^{-2} rad., and the analytical result can follow the tendency. On the other hand, for Specimen CWBS with anchorage, the shear deformation in the 1st story increased with increasing R, while that in the 2nd story decreased in the test results. The analytical results showed good agreement with the test results, using a shear stiffness reduction factor β_u calculated by Eq. 8 in section 3.2.

In Specimens CWAF with flexural failure, the shear deformation in the 1st story in the analysis was slightly larger than that in the test before R of 0.5 x 10^{-2} rad. However, in Specimens CWAF and CWBF, the transition of the ratios of each deformation component in the analysis showed good agreement with that in the test after R of 0.75 x 10^{-2} rad.

Thus, it is clarified that the analytical results such as backbone curves, hysteretic characteristics and the transitions of deformation components showed good agreement with the test results. Namely, it is conformed that the analytical model based on TVLE model for CES shear walls proposed in this paper is effective to apply for the nonlinear analysis of CES structures. .

5. Conclusions

In this study, the restoring force characteristics model of CES shear walls using simplified longitudinal bars arrangement in the wall examined to apply the structural performance evaluation method of CES building. The following conclusions can be drawn.

1) The initial stiffness of boundary columns subjected to tension should be reduced to half of steel stiffness in Axial-Stiffness model because bond resistance between steel and concrete in the boundary column cannot be expected.
2) Takeda-Slip model is effective for the hysteretic characteristics of shear deformation component.
3) In the CES shear wall, the effects of the different analytical model of axial restoring force characteristic in the wall on the backbone curve and hysteretic characteristics was small.
4) Analytical results using the restoring force characteristics model proposed in this paper show good agreement with test results on CES shear walls

6. References

Shunsuke SUGANO, Study on Restoring Characteristics of Reinforced Concrete members, *Concrete Journal*, Vol.11, No.2, pp1-9, 1973 (in Japanese)

Suguru SUZUKI, Tomoya MATSUI, Hiroshi KURAMOTO, A Fundamental Study on Structural Performance of CES Shear Walls with Different Anchorage Condition of Wall Reinforcing Bars, *Proceedings of 15WCEE*, 2012.9

Suguru SUZUKI, Hiroshi KURAMOTO, Tomoya MATSUI, Non-Linear FEM Analysis for CES Shear Walls, *Proceedings of 10th U.S. National Conference on Earthquake Engineering,* pp.1533-1540, 2014.7

Toshimi KABEYASAWA, Shunsuke OTANI, Hiroyuki AOYAMA, Nonlinear Dynamic Analyses of R/C Wall-Frame Structures, *Proceedings of the Japan, Concrete Institute*, Vol.5, pp.213-216, 1983.7 (in Japanese)